Control Moment Gyros as Space-Robotics Actuators

Daniel Brown[1]
Cornell University, Ithaca, New York, 14850

Control moment gyros (CMGs) are an energy-efficient means of reactionless actuation. CMGs operate by gimbaling a high-speed rotor to change the momentum of a base body. We investigate a robotic linkage actuated by scissored-pair CMGs. Scissored pairs constrain the output torque from the CMGs to act along the joint axis, eliminating undesirable gyroscopic reaction torques. This work compares the energy required to actuate a robotic linkage with either CMGs or direct drive motors. We show that the CMG power is equal to the direct-drive power for a large range of gimbal inertias and peak gimbal angles. The transverse rate does not independently affect this result. We find that the scissored pair's peak gimbal rate is a ratio of body acceleration to body rate. The equations of motion for an n-link robot with CMGs are presented in a recursive form for easy implementation in software. The results for a one-link robot extend easily to two-link robots with orthogonal joint axes when the peak body rate and peak gimbal angle are adjusted to account for the influence of neighboring links. CMGs surprisingly outperform direct drive for a two-link robot with parallel joint axes when the joints rotate with opposite sign, as in reaching tasks; although the reverse is true when the joints act in unison. These differences arise because CMGs produce body torques with a zero-torque boundary condition at the joint, whereas direct drive produces joint torques.

I. Introduction

REACTIONLESS actuation of a robotic assembly on a spacecraft provides several advantages over typical actuation methods [1]. A reactionless system decouples the attitude control system (ACS) from the dynamics of the robotic arm. System-level pointing performance can be improved by removing the known disturbances created by a robotic arm. The robot arm may include the sensors
or camera being pointed. For such a configuration, rapid robotic movements do not impart low-frequency disturbances that might excite structural vibrations. Another benefit of reactionless robotics is that the agility required of a specific subsystem need not be applied to the satellite as a whole, reducing the peak ACS torques when used with the robot. This work explores possible power-efficiency advantages of a reactionless robot without making assumptions about the ACS power savings. Power-efficient control moment gyros (CMGs) produce a torque directly on a body without transmitting that torque through neighboring joint axes. We compare the energy used by a robot linkage actuated with direct drive motors acting on the joints to that of an identical system actuated by CMGs. We also give novel results on differences between the two systems that arise from joint axis arrangements because CMGs apply torques directly to each body, not through the joints.

A spinning body resists change in both the magnitude and the direction of spin, i.e., the change in angular momentum is equal to the applied moments. Momentum control of a body uses the embedded momentum of a spinning rotor to produce an internal torque that causes the rest of the body to rotate in such a way that the system's angular momentum stays constant. A body that uses momentum control can reorient without propellant and without changing its system net angular momentum, valuable traits in spacecraft applications. The internal momentum is either a fixed-axis, variable-speed rotor (reaction wheel) or a gimbaled-axis, constant-speed rotor (CMG), or both (variable-speed CMGs) [2].

A reaction wheel assembly (RWA) changes its rotor speed only. The spin axis is fixed to the satellite. The approximate energy cost of using an RWA of inertia I_r is the change in the kinetic energy of the rotor.

[1] Graduate student researcher, Mechanical and Aerospace Engineering, 138 Upson Hall, AIAA student member.

$$\Delta E_r = \frac{1}{2} I_r \left(\omega_2^2 - \omega_1^2 \right) \tag{1}$$

where the initial and final speeds of the rotor (ω_1, ω_2) are taken relative to the satellite reference frame. In spite of the added energy cost, reaction wheels have been used extensively due to their simplicity, reliability, and strong flight heritage. In contrast, the CMG uses a constant-speed rotor on a gimbaled axis. Its rotor's kinetic energy changes only insignificantly (e.g. in response to low-speed base motions). To first order, the change in angular momentum is given by the gimbal rate crossed with the rotor momentum, resulting in a torque perpendicular to both the gimbal and the rotor axes (see Fig. 1).

$$\boldsymbol{\tau}_C = -\dot{\phi}\hat{\boldsymbol{g}} \times \boldsymbol{h}_r \tag{2}$$

CMGs also have an important flight heritage, especially for producing large torques required of large structures such as ISS or MIR [3]. Much recent attention has focused on smaller CMGs for use on small satellites [4, 5]. This paper aims to encourage further development of small CMGs by highlighting their potential application to robotics.

Some energy is used for CMG driven maneuvers—at least as much as the change in the satellite's kinetic energy. We explore how much energy is used by a CMG with a constant speed rotor, limiting ourselves to scissored-pair, single-gimbal CMGs throughout this study. Comparisons of RWAs and CMGs have previously shown the power benefits of using CMGs, both in attitude control and specifically for robotic applications [6].

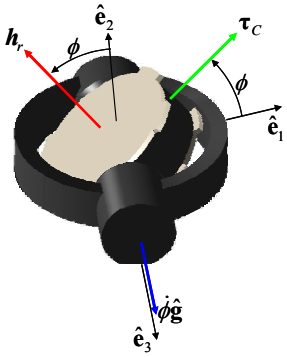

Figure 1. CMG vectors and scalars defined.

Robot arms usually use electric motors at the joints. A proposed bifocal relay telescope uses CMG attitude control on one member, and connects the other member with a joint motor [7]. CMG-actuated robotic linkages are a recent idea and have been proposed for vibration and slew control of a large truss [8] and three-degrees-of-freedom control of a coelostat telescope [9]. The proposed CMG-actuated robots use scissored pairs of CMGs—also referred to as V-gyros or twin-gyros [10-12]. Scissored pairs produce torque about a single axis by using mirrored gimbal angles to cancel unwanted torque on the body. Cross coupling torques acting on the gimbal motors that result from body motion can be cancelled internally to reduce gimbal torque [12-14]. The present work considers first a single-link robot to create an intuitive foundation and provide useful equations for sizing CMGs. We compare CMGs to direct-drive actuation--the likely competing technology for robotic actuation--for a one- and two-link robotic arm. We give an explanation for novel and counter-intuitive results for which CMGs outperform direct drive in a planar two-link arm.

II. CMG Dynamics

A. Isolated CMG

This section develops the equations of motion for a single CMG. Similar equations have been developed elsewhere [15], but the following first-principles derivations clarify the assumptions made and help establish notation before combining two CMGs into a scissored pair.

Consider a Newtonian frame denoted by N, a body-fixed frame B, and the CMG gimbal-fixed frame G. The CMG's angular momentum vector about its center of mass, $\boldsymbol{h}_c$, is the combined momentum of the gimbal and the rotor:

$$\begin{aligned} \boldsymbol{h}_c &= \boldsymbol{I}_g \cdot \boldsymbol{\omega}^{\mathrm{G/N}} + \boldsymbol{I}_r \cdot \boldsymbol{\omega}^{\mathrm{R/N}} \\ &= \boldsymbol{I}_g \cdot \left(\boldsymbol{\omega}^{\mathrm{G/B}} + \boldsymbol{\omega}^{\mathrm{B/N}} \right) + \boldsymbol{I}_r \cdot \left(\boldsymbol{\omega}^{\mathrm{R/G}} + \boldsymbol{\omega}^{\mathrm{G/B}} + \boldsymbol{\omega}^{\mathrm{B/N}} \right) \\ &= \boldsymbol{I}_{gr} \cdot \left(\boldsymbol{\omega}^{\mathrm{G/B}} + \boldsymbol{\omega}^{\mathrm{B/N}} \right) + \boldsymbol{h}_r \end{aligned} \tag{3}$$

For a constant speed rotor, the time derivative of Eq. (3) taken in the N frame is

$$\overset{\mathrm{N}}{\boldsymbol{h}}_c = \boldsymbol{I}_{gr} \cdot \left(\overset{\mathrm{G}}{\boldsymbol{\omega}}^{\mathrm{G/B}} + \overset{\mathrm{B}}{\boldsymbol{\omega}}^{\mathrm{B/N}} - \boldsymbol{\omega}^{\mathrm{G/B}} \times \boldsymbol{\omega}^{\mathrm{B/N}} \right) + \left(\boldsymbol{\omega}^{\mathrm{G/B}} + \boldsymbol{\omega}^{\mathrm{B/N}} \right) \times \left(\boldsymbol{I}_{gr} \cdot \left(\boldsymbol{\omega}^{\mathrm{G/B}} + \boldsymbol{\omega}^{\mathrm{B/N}} \right) + \boldsymbol{h}_r \right) \tag{4}$$

where the following shorthand is used to indicate a vector derivative:

$$\frac{\overset{\mathrm{N}}{d}}{dt} \boldsymbol{\omega} = \overset{\mathrm{N}}{\boldsymbol{\omega}} \tag{5}$$

For the analysis and simulation, the CMG inertia $\boldsymbol{I}_{gr}$ is constant in any frame as for a spherical body.

$$\boldsymbol{I}_g + \boldsymbol{I}_r = \boldsymbol{I}_{gr} = I_{gr} \boldsymbol{1} \tag{6}$$

This simplification clarifies the analytical results by eliminated various minor terms in the equation and reduces the number of free parameters in the simulations. We justify this choice for a physical system by noting that $\boldsymbol{I}_{gr}$ combines the gimbal support structure and attached framework and motors with the rotor. The gimbal rate and acceleration may be written in terms of the gimbal angle ϕ using an over dot to denote the time derivative of a scalar.

$$\boldsymbol{\omega}^{\mathrm{G/B}} = \dot{\phi} \hat{\boldsymbol{g}} \tag{7}$$

$$\overset{\mathrm{G}}{\boldsymbol{\omega}}^{\mathrm{G/B}} = \ddot{\phi} \hat{\boldsymbol{g}} \tag{8}$$

Combining Eqs. (6) to (8) with Eq. (4) results in a more usable form:

$$\overset{\mathrm{N}}{\boldsymbol{h}}_c = I_{gr} \cdot \left(\ddot{\phi} \hat{\boldsymbol{g}} + \overset{\mathrm{B}}{\boldsymbol{\omega}}^{\mathrm{B/N}} - \dot{\phi} \hat{\boldsymbol{g}} \times \boldsymbol{\omega}^{\mathrm{B/N}} \right) + \left(\dot{\phi} \hat{\boldsymbol{g}} + \boldsymbol{\omega}^{\mathrm{B/N}} \right) \times \boldsymbol{h}_r \tag{9}$$

The time derivative of the angular momentum must be equal to the external torques. The torques acting on the CMG are the supplied gimbal torque and the torque reacted onto the body. We neglect friction, electromagnetic, and flexible effects, instead focusing on the dynamics of the system. The gimbal torque always acts about the gimbal axis whereas the direction of torque reacted onto the body varies. Even for a stationary body ($\boldsymbol{\omega}$=0), the CMG torque on the body will change based on the gimbal angle (Eq. (2)).

Adapting to changing CMG output torque is among the biggest challenges of CMG-based attitude-control system design due to singularities [16]. Singularities arise when the possible output torques cannot produce the desired torque. For the system under investigation here, the desired torque is always along the joint axis. We use a scissored pair to constrain the torque output to act only along the joint axis.

B. Scissored Pair

In a scissored-pair, two CMGs with parallel gimbal axes maintain equal-magnitude and opposite-sign gimbal angles (Fig. 2). Singularities occur only if the commanded torque exceeds the capability of the scissored pair in magnitude or if the momentum stored in the pair is at a maximum. These saturation singularities occur in any actuator. Scissored pairs also have a simple zero-angular-momentum configuration, important for rotor spin-up and ensuring that motion of other links does not induce unwanted gyroscopic torque. We have also shown elsewhere how the base-rate effects can be reduced in a scissored pair through a mechanical coupling that enforces the gimbal angle constraint [13]. While we do not explore the application of a single CMG for each link, we speculate that there may be some benefit to be gained by using them in this way; we set aside these issues for future work.

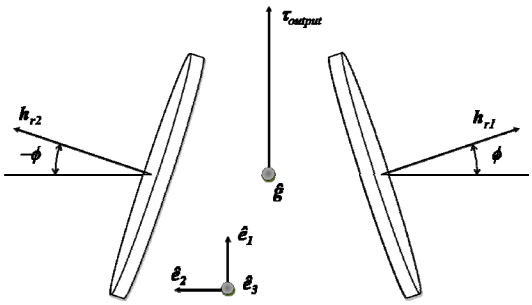

Figure 2. Scissored-pair kinematics.

The magnitude of the gimbal torque for the first CMG is found by taking the dot product of $\hat{\boldsymbol{g}}$ with Eq. (9). To distinguish between the two CMGs, a subscript 1 or 2 is used.

The direction of the rotor momentum is different for each CMG, even though the magnitude is constant, so that $\boldsymbol{h}_{r1} \neq \boldsymbol{h}_{r2}$.

$$\tau_{g1} = I_{gr}\ddot{\phi} + I_{gr}\,{}^{\mathrm{B}}\boldsymbol{\omega}^{\mathrm{B/N}} \cdot \hat{\boldsymbol{g}} + \left(\boldsymbol{\omega}^{\mathrm{B/N}} \times \boldsymbol{h}_{r1}\right) \cdot \hat{\boldsymbol{g}} \tag{10}$$

For the other CMG, we replace ϕ with $-\phi$.

$$\tau_{g2} = -I_{gr}\ddot{\phi} + I_{gr}\,{}^{\mathrm{B}}\boldsymbol{\omega}^{\mathrm{B/N}} \cdot \hat{\boldsymbol{g}} + \left(\boldsymbol{\omega}^{\mathrm{B/N}} \times \boldsymbol{h}_{r2}\right) \cdot \hat{\boldsymbol{g}} \tag{11}$$

The control volumes shown in Fig. 3 show that the net applied torque, τ_A, is equal to the difference between the two gimbal torques when using a mechanical coupling to enforce the mirror symmetry of the scissored pair.

$$\tau_A = \tau_{g1} - \tau_{g2} \tag{12}$$

$$\tau_A = 2I_{gr}\ddot{\phi} + \left(\boldsymbol{\omega}^{\mathrm{B/N}} \times \left(\boldsymbol{h}_{r1} - \boldsymbol{h}_{r2}\right)\right) \cdot \hat{\boldsymbol{g}} \tag{13}$$

$$\tau_A = 2I_{gr}\ddot{\phi} - \boldsymbol{\omega}^{\mathrm{B/N}} \cdot 2h_r \cos\phi \hat{\boldsymbol{e}}_1 \tag{14}$$

The first term corresponds to rotating the gimbal. The latter term accounts for the body rate and may be referred to as the base-rate effect. The base-rate effect plays a significant role in energy costs of CMGs. The rotor momentum is usually large relative to the gimbal inertia and accelerations, with the latter limited by the gimbal motor. A simplified expression for gimbal torque is:

$$\tau_A \approx -\boldsymbol{\omega}^{\mathrm{B/N}} \cdot 2h_r \cos\phi \hat{\boldsymbol{e}}_1 \tag{15}$$

The power used by the CMGs for a maneuver is determined using gimbal torque times gimbal rate.

$$P = \left|\tau_A \dot{\phi}\right| \tag{16}$$

This expression neglects losses due to friction and electromagnetic inefficiencies under the likely assumption that the gimbal torque *per se* drives the power design in an agile application. Friction losses may make CMGs an inefficient choice for a generally quiescent system. This study does not distinguish between positive or negative power since both require energy from the spacecraft power system. The sign would matter in a case where the spacecraft power system efficiently recovered this energy expenditure in a regenerative fashion, e.g. using the gimbal motor as a generator. We assume that such an architecture is not in place for purposes of this study. Here, power is independent of the sign of gimbal torque and gimbal rate. Therefore we consider the absolute value of power in our comparisons.

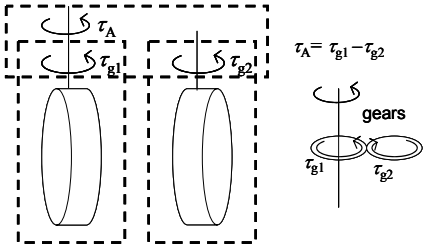

Figure 3. Gimbal torques for a scissored pair.

III. Single Link Robot

We first derive an analytical expression for power use for a single link powered by either a scissored-pair of CMGs or direct drive and show both use the same power. In this work, the robot attaches to a stationary base, i.e. the satellite is sufficiently large and slow to neglect the base dynamics. We consider specifically agile robotic applications with motions up to 1 rad/s—rates that favor a reactionless robot over a fixed spacecraft. We simulate a single-link robot to extend the results of the analysis to include larger gimbal inertias and a non-zero transverse rate of the base.

A. Single Link Analysis

As before, we derive the equations associated with the general case and apply reasonable assumptions to gain intuition about the system. The motion of a single link may be described in terms of the angular momentum:

$$\boldsymbol{H} = \boldsymbol{I}_b \cdot \boldsymbol{\omega}^{\mathrm{B/N}} \tag{17}$$

The angular momentum derivative is

$$\overset{\mathrm{N}}{\boldsymbol{H}} = \boldsymbol{I}_b \cdot \overset{\mathrm{B}}{\boldsymbol{\omega}}{}^{\mathrm{B/N}} + \boldsymbol{\omega}^{\mathrm{B/N}} \times \left(\boldsymbol{I}_b \cdot \boldsymbol{\omega}^{\mathrm{B/N}} \right) \tag{18}$$

The direct drive torque acting on the joint axis $\hat{\boldsymbol{e}}_1$ is given by

$$\tau_{DD} = \boldsymbol{I}_b \cdot \overset{\mathrm{B}}{\boldsymbol{\omega}}{}^{\mathrm{B/N}} \cdot \hat{\boldsymbol{e}}_1 + \left(\boldsymbol{\omega}^{\mathrm{B/N}} \times \left(\boldsymbol{I}_b \cdot \boldsymbol{\omega}^{\mathrm{B/N}} \right) \right) \cdot \hat{\boldsymbol{e}}_1 \tag{19}$$

CMGs actuate the robot via internal momentum exchange. The total momentum of the link and CMGs is

$$\begin{aligned} \boldsymbol{H} &= \boldsymbol{h}_{link} + \boldsymbol{h}_{CMG1} + \boldsymbol{h}_{CMG2} \\ \boldsymbol{H} &= \boldsymbol{I}_{link} \cdot \boldsymbol{\omega}^{\mathrm{B/N}} + \boldsymbol{I}_{gr} \cdot \left(\boldsymbol{\omega}^{\mathrm{G1/B}} + \boldsymbol{\omega}^{\mathrm{B/N}} \right) + \boldsymbol{h}_{r1} + \boldsymbol{I}_{gr} \cdot \left(\boldsymbol{\omega}^{\mathrm{G2/B}} + \boldsymbol{\omega}^{\mathrm{B/N}} \right) + \boldsymbol{h}_{r2} \end{aligned} \tag{20}$$

The sum of the rotor momenta takes the form (Fig. 2)

$$\boldsymbol{h}_{r1} + \boldsymbol{h}_{r2} = 2h_r \sin\phi \hat{\boldsymbol{e}}_1 \tag{21}$$

The momentum of the gimbals relative to the body cancels because the gimbal rates are opposite. Without loss of generality, we combine the inertias of the link and CMGs into the inertia dyadic $\boldsymbol{I_b}$.

$$\boldsymbol{I}_b = \boldsymbol{I}_{link} + 2\boldsymbol{I}_{gr} \tag{22}$$

With this substitution the total momentum of Eq. (20) reduces to

$$\boldsymbol{H} = \boldsymbol{I}_b \cdot \boldsymbol{\omega}^{\mathrm{B/N}} + 2h_r \sin\phi_i \hat{\boldsymbol{e}}_{i1} \tag{23}$$

The derivative of the angular momentum is

$$\overset{\mathrm{N}}{\boldsymbol{H}} = \boldsymbol{I}_b \cdot \overset{\mathrm{B}}{\boldsymbol{\omega}}{}^{\mathrm{B/N}} + \boldsymbol{\omega}^{\mathrm{B/N}} \times \left(\boldsymbol{I}_b \cdot \boldsymbol{\omega}^{\mathrm{B/N}} \right) + 2h_r \dot{\phi} \cos\phi \hat{\boldsymbol{e}}_1 + \boldsymbol{\omega}^{\mathrm{B/N}} \times 2h_r \sin\phi \hat{\boldsymbol{e}}_1 \tag{24}$$

The projection of Eq. (24) onto the joint axis $\hat{\boldsymbol{e}}_1$ must be zero due to the absence of joint torques for a CMG actuated robot. The gimbal rate and the body rate are determined by the following:

$$0 = \boldsymbol{I}_b \cdot \overset{\mathrm{B}}{\boldsymbol{\omega}}{}^{\mathrm{B/N}} \cdot \hat{\boldsymbol{e}}_1 + \boldsymbol{\omega}^{\mathrm{B/N}} \times \left(\boldsymbol{I}_b \cdot \boldsymbol{\omega}^{\mathrm{B/N}} \right) \cdot \hat{\boldsymbol{e}}_1 + 2h_r \dot{\phi} \cos\phi \tag{25}$$

In our simulations below, the gimbal rates are determined directly from the joint rates and accelerations.

We next show an equivalent power cost for the CMGs and direct drive. Consider a single link that rotates about a fixed joint axis with an angular velocity $\dot{\theta}\hat{\boldsymbol{e}}_1$. The direct-drive torque is

$$\tau_{DD} = I_b \ddot{\theta} \tag{26}$$

The power is the product of the torque and rate.

$$P_{DD} = I_b \ddot{\theta}\dot{\theta} \tag{27}$$

With the same geometry and motion for the scissored-pair actuated link, Eq. (25) determines the gimbal rate for a given link rotation:

$$\dot{\phi} = \frac{-I_b \ddot{\theta}}{2h_r \cos\phi} \tag{28}$$

Differentiating gives an expression for gimbal acceleration:

$$\ddot{\phi} = \frac{-I_b \dddot{\theta} + 2h_r \dot{\phi}^2 \sin\phi}{2h_r \cos\phi} \tag{29}$$

For Eq. (15) we assume the gimbal acceleration is small. Equation (29) shows that the body acceleration, jerk, and inertia must be small, and the gimbal angle avoids saturation singularities for this to be true.

The gimbal torque with the angular velocity about one axis is:

$$\tau_A = 2I_{gr}\ddot{\phi} - 2\dot{\theta}h_r \cos\phi \tag{30}$$

The gimbal-motor power is the product of the torque in Eq. (30) and the gimbal rate in Eq. (28).

$$P_{CMG} = \left(2I_{gr}\ddot{\phi} - 2\dot{\theta}h_r \cos\phi\right)\frac{-I_b\ddot{\theta}}{2h_r \cos\phi} \tag{31}$$

When the gimbal inertia and acceleration are small, the CMG power simplifies to:

$$P_{CMG} \approx I_b \ddot{\theta}\dot{\theta} \tag{32}$$

This is the same as the direct-drive power in Eq. (27). An interesting consequence of this result is that the effect of gimbal angle in a scissored pair is removed from the power equation. A non-zero-momentum set point would not affect the power usage except as needed to maintain the torque in Eq. (30). The rotor momentum is also absent from Eq (32). One source of uncertainty in the rotor momentum is a constant gimbal-angle offset due to misalignment of the gimbal angles in a scissored pair. Therefore a constant gimbal-angle misalignment will not affect CMG power.

We also note that this result does not depend on torque amplification. Any decrease in gimbal torque due to torque amplification will be offset by a decrease in velocity, and *vice versa*. Furthermore, leveraging torque amplification in CMGs requires a gimbal rate greater than the body rate [17]. However agile systems may have performance requirements that contradict this requirement. To show this, we use conservation of momentum about the joint axis to determine the maximum gimbal angle, ϕ_{peak}.

$$2h_r \sin\left(\phi_{peak}\right) = I_b \dot{\theta}_{peak} \tag{33}$$

In other words, ϕ_{peak} measures how conservative the CMGs are sized for a given system. This equation with Eq. (28) provides a bound on the gimbal rate:

$$\left|\dot{\phi}\right| \le \frac{\ddot{\theta}_{peak}}{\dot{\theta}_{peak}} \tan\left(\phi_{peak}\right) \tag{34}$$

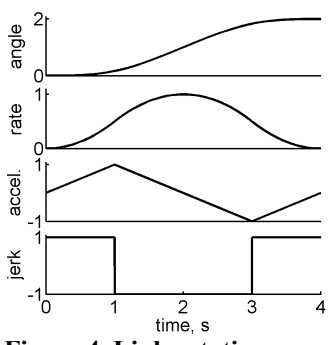

Figure 4. Link rotation.

Sizing a CMG to provide torque amplification may artificially limit ϕ_{peak}. However, such a system may offer other advantages in accuracy, bandwidth, and motor size.

This analysis demonstrates that internal momentum exchange is not inherently inefficient relative to direct drive. Using CMGs to rotate a robot link does not significantly increase the power cost of the system. The CMG system does add complexity and rotor losses to the robotic system, but it provides the valuable opportunity for reactionless actuation.

B. Single-Link Simulations

In this section, we simulate a single link actuated by either direct drive or a scissored pair of CMGs as discussed above. The link motions are prescribed to

facilitate comparison between direct drive and scissored pairs without confounding factors from a particular control algorithm. The link is rotated through a given angle in least time, subject to maximum rate, acceleration, and jerk requirements (see Fig. 4). We arbitrarily select a maximum link rate, acceleration, and jerk of 1 (rad/s, rad/s^2, rad/s^3), and the link rotates 2 rad. The angle profile shown in Fig. 4 is achieved via the following relationships among total link rotation and maximum rate, acceleration, and jerk:

$$\omega_{\max} \cdot j_{\max} = a_{\max}^2 \tag{35}$$

$$\Delta\theta = \omega_{\max}\left(\frac{\omega_{\max}}{a_{\max}} + \frac{a_{\max}}{j_{\max}}\right) \tag{36}$$

$$\Delta t = 4\, a_{\max} \big/ j_{\max} \tag{37}$$

For a given trajectory, we calculate the torque and power required by the direct-drive and CMG actuators, and integrate power over time to obtain the total energy used by each actuation method. We calculate the percent energy difference (*PED*) of the scissored pair relative to direct drive:

$$PED = \frac{E_{CMG} - E_{DD}}{E_{DD}} \times 100 \tag{38}$$

1. Gimbal inertia variation

In the first simulation, we explore the contribution of $2I_{gr}\ddot{\phi}$ to gimbal power (Eq. (31)) We vary both the gimbal inertia, I_{gr} and the rotor momentum—or equivalently ϕ_{peak}. This analysis assumes that the gimbal inertia does not increase the body inertia; i.e., the sum in Eq. (22) is constant for these simulations. The only effect gimbal inertia has on energy use independent of the total body inertia is its contribution to the gimbal torque of Eq. (14). The baseline parameters for all single-link simulations are given in Table 1. We used 30 evenly spaced values for ϕ_{peak} and I_{gr} over the ranges specified in Table 1. The results are shown in Fig. 5 with the baseline case indicated with a white dot. It can be shown using Eqs. (28) and (29) that I_{gr}*(cosϕ)$^{-4}$ enters into the expression for gimbal power—explaining the sharp rise in power as the CMGs approach a singularity. The flat region indicates a large design space for ϕ_{peak} and I_{gr} available to robot designers interested in CMGs.

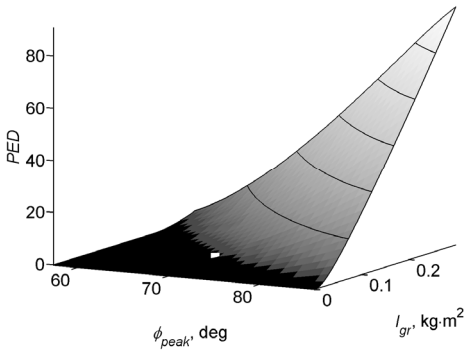

Figure 5. Gimbal inertia and peak gimbal angle effect on CMG energy use.

Table 1. Parameters for single-link simulation.

	$\Delta\theta$, deg	$\omega_{\max}$, s^{-1}	$a_{\max}$, s^{-2}	$j_{\max}$, s^{-3}	$\boldsymbol{I}_b$, kg·m^2	h_r, N·m·s	ϕ_{peak}, deg	I_{gr}, kg·m^2	*PED*, %
Baseline	115	1	1	1	1·***1***	0.53	70	0.1	1.0
Gimbal study	"	"	"	"	"	0.50—0.59	57—86	0—0.3	-0.1—91
Base rate study	"	1 & 0.5	"	"	0.8—1.2	0.44—0.63	63—78	0.1	ave 1.2

2. Transverse rate

A robotic link may be attached to a moving spacecraft base or other robotic links. The second simulation assumes that the spacecraft is rotating about a transverse axis at a constant rate throughout the maneuver. The assigned body rate is given by

$$\boldsymbol{\omega}^{\mathrm{B/N}} = \begin{bmatrix} \dot{\theta} & \omega_2 & \omega_3 \end{bmatrix}^T \tag{39}$$

where ω_2 and ω_3 are constants such that total transverse rate is less than 0.5 rad/s. We also vary the link inertia to ensure the off-axis rotation fully contributes to the dynamics. In a physical inertia, the maximum principal inertia cannot be greater than the sum of the other two principal inertias. The inertia matrix must also be symmetric. Peck describes a method of simulating a distribution of random inertia matrices [18] that selects the principal inertias and randomly rotates this diagonal matrix. In this work the principal inertias are drawn from the sum of uniform distributions to explore the parameter space, not to perform an exhaustive search. The rotor momentum is determined from conservation of momentum as per Eq. (33) using $I_b = \boldsymbol{I}_1 \cdot \hat{\boldsymbol{e}}_1 \cdot \hat{\boldsymbol{e}}_1$ and ϕ_{peak} = 70 deg. The range of values of ϕ_{peak} given in Table 1 reflects the angular momentum from the gimbals and asymmetry of the inertia dyadic about the joint axis. The results for 1000 simulations are shown in Fig. 6. The total transverse rotation appears to affect the performance of the CMG robot (Fig. 6a). However, by plotting the percent energy difference *PED* against ϕ_{peak} and the ratio of gimbal inertia to the body inertia, we reproduce the basic shape of Fig. 5. We conclude that transverse rate does not affect the energy used by a scissored pair beyond its influence on ϕ_{peak} and the relative sizes of the gimbal and body inertias.

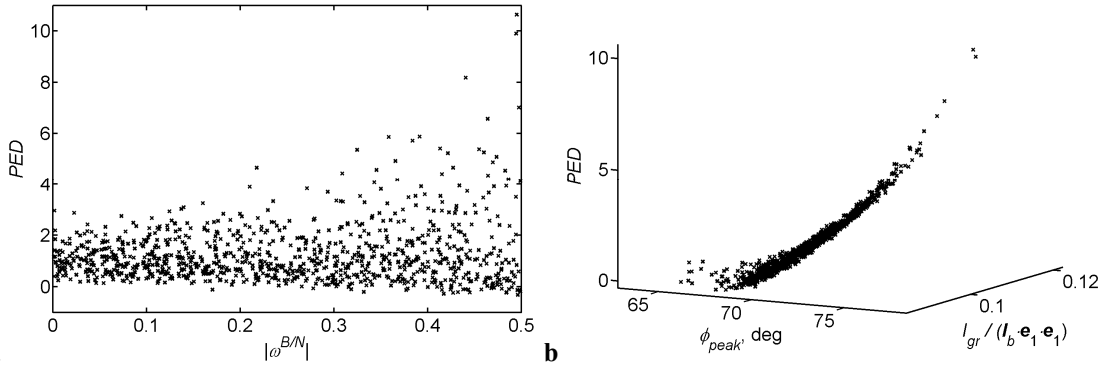

Figure 6. Effect of transverse rate. a. *PED vs. total transverse rate.* **b.** *PED vs.* ϕ_{peak} *and* I_{gr}/I_b.

A robot with just one joint provides several important lessons for designing CMGs for robotics. Derivations and simulation confirm that CMG actuation does not add energy costs above those of direct-drive actuation in reasonable operating regimes. Undersized CMGs and bulky gimbals add to the energy costs, but not necessarily off-axis rotations. Electrical or mechanical efficiencies—including the cost of maintaining the CMG rotor at a constant speed in the presence of drag losses—also add to the energy costs but have not been considered in this study. The transverse rate of a link appears not to directly affect energy costs, though it may influence other factors. When not operating near singularities, power is independent of the rotor's angular momentum, including gimbal angle offsets, and the gimbal rates. We also give a simple expression for the peak gimbal rate based on performance parameters of the robot. Taken together, these results provide a straightforward means of sizing CMGs for a particular robot application.

IV. Multilink Robot

We use Kane's equations [19, 20], equivalent to the principle of virtual power in this formulation [21], to derive the equations of motion for n-link robotic systems with either direct-drive or scissored-pair actuation. We use the following form of Kane's equations to develop the equations of motion.

$$\sum_{i=1}^{n} \left(m_i \overset{\mathrm{N}}{\boldsymbol{v}}_i - \boldsymbol{F}_i^a \right) \cdot \frac{\partial \boldsymbol{v}_i}{\partial \dot{q}_k} + \sum_{i=1}^{n} \left(\overset{\mathrm{N}}{\boldsymbol{H}}_i - \boldsymbol{M}_i^a \right) \cdot \frac{\partial \boldsymbol{\omega}^{\mathrm{B}i/\mathrm{N}}}{\partial \dot{q}_k} = 0 \text{ for } k = 1..n \tag{40}$$

The number of links is n, i sums over each link, and k indexes the generalized coordinates. There are n generalized coordinates for a grounded serial linkage with revolute joints. The applied forces and moments are $\mathbf{F}^a$ and $\mathbf{M}^a$, with a subscript indicating the link being acted on. The partial derivatives in Eqs. (40) are known as partial velocities and indicate the component of the velocity or rate aligned with the appropriate generalized coordinate. The velocities and rates are taken with respect to an inertial frame. Each body frame is denoted Bi, or i for short, with the basis vector $\hat{\mathbf{e}}_{i1}$ aligned with the i^{th} joint axis. The zero link is taken as the nonrotating N frame. We use the angle of

rotation of each link about its joint axis as the generalized coordinates, q_i. We do not write one large expression for the equations of motion; rather we separate the pieces into blocks that can be assembled for any number of links. Recursive expressions for each term allow additional arms to be added using the same block of code with another joint-angle command. Since we use prescribed motion, we do not include a feedback term. Including feedback requires an expression for the mass matrix, a simple exercise in algebra and index accounting that we do not include here. A schematic of the code structure for the direct drive simulation is shown in Fig. 7.

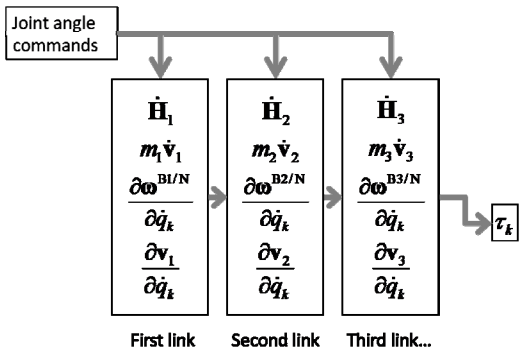

Figure 7. Code structure for n-link robot with direct drive.

The angular velocity of link i with respect to the Newtonian frame is defined recursively as:

$$\boldsymbol{\omega}^{Bi/N} = \dot{q}_i \hat{\boldsymbol{e}}_{i1} + \boldsymbol{\omega}^{Bi-1/N} \tag{41}$$

The angular acceleration is also given recursively:

$$\overset{i}{\boldsymbol{\omega}}{}^{Bi/N} = \ddot{q}_i \hat{\boldsymbol{e}}_{i1} - \dot{q}_i \hat{\boldsymbol{e}}_{i1} \times \boldsymbol{\omega}^{Bi-1/N} + \overset{i-1}{\boldsymbol{\omega}}{}^{Bi-1/N} \tag{42}$$

From Eq. (41), the partial angular velocity term in Eqs. (40) can be concisely written.

$$\frac{\partial \boldsymbol{\omega}^{Bi/N}}{\partial \dot{q}_k} = \begin{cases} \hat{\boldsymbol{e}}_{k1} & k \le i \\ 0 & k > i \end{cases} \tag{43}$$

We let $\boldsymbol{I}_i$ denote the inertia of link i and its actuator. Differences between direct-drive and scissored-pair inertias are identical to changing the body inertia. We set aside the question of the relative mass of a scissored pair and a direct-drive motor and gearbox but acknowledge that it would receive some attention in a trade study of a specific application. The angular momentum of link i and its derivative are given in Eqs. (17) and (18). Appropriate indexing of the latter equation yields:

$$\overset{N}{\boldsymbol{H}}_i = \boldsymbol{I}_i \overset{i}{\boldsymbol{\omega}}{}^{Bi/N} + \boldsymbol{\omega}^{Bi/N} \times \boldsymbol{I}_i \boldsymbol{\omega}^{Bi/N} \tag{44}$$

The position vector of a single link could easily be couched in the inertia. For an n-link mechanism, we define $\boldsymbol{l}_i$ as the vector from the i-frame origin to the $i+1$-frame origin, and the vector from the i-frame origin to the center of mass of link i is $\mathbf{r}_i$. With these definitions, the position and velocity of the i^{th} link relative to the inertial frame origin are written recursively as:

$$\boldsymbol{r}_{i/N} = \sum_{j=1}^{i-1} \boldsymbol{l}_j + \boldsymbol{r}_i \tag{45}$$

$$\boldsymbol{v}_{i/N} = \sum_{j=1}^{i-1} \boldsymbol{\omega}^{Bj/N} \times \boldsymbol{l}_j + \boldsymbol{\omega}^{Bi/N} \times \boldsymbol{r}_i \tag{46}$$

The corresponding partial velocities are:

$$\frac{\partial \boldsymbol{v}_{i/N}}{\partial \dot{q}_k} = \begin{cases} \hat{\boldsymbol{e}}_{B_k 1} \times \left(\boldsymbol{r}_i + \sum_{j=k}^{i-1} \boldsymbol{l}_j \right) & i \ge k \\ 0 & i < k \end{cases} \tag{47}$$

where it is understood that $\boldsymbol{l}_j$ no longer enters the equation when $i=k$,. The acceleration of link i is

$$\overset{\mathrm{N}}{\boldsymbol{v}}_{i/\mathrm{N}} = \sum_{j=1}^{i-1}\left\{\overset{j}{\boldsymbol{\omega}}^{\mathrm{B}j/\mathrm{N}}\times\boldsymbol{l}_j + \boldsymbol{\omega}^{\mathrm{B}j/\mathrm{N}}\times\left(\boldsymbol{\omega}^{\mathrm{B}j/\mathrm{N}}\times\boldsymbol{l}_j\right)\right\} + \overset{\mathrm{N}}{\boldsymbol{\omega}}^{\mathrm{B}i/\mathrm{N}}\times\boldsymbol{r}_i + \boldsymbol{\omega}^{\mathrm{B}i/\mathrm{N}}\times\left(\boldsymbol{\omega}^{\mathrm{B}i/\mathrm{N}}\times\boldsymbol{r}_i\right) \tag{48}$$

With no applied forces in the problem, $\mathbf{F}^a$=0. The applied moments on link *i* for direct-drive are

$$\boldsymbol{M}_i^a = \tau_i\hat{\boldsymbol{e}}_{i1} - \tau_{i+1}\hat{\boldsymbol{e}}_{i+1,1} \tag{49}$$

The applied moments become much less cumbersome after summing over all the links. The k^{th} equation from Eqs. (40) has a single torque term after taking the sum of applied moments dotted with the partial angular velocities.

$$\sum_{i=1}^{N}\boldsymbol{M}_i^a\cdot\frac{\partial\boldsymbol{\omega}^{\mathrm{B}i/\mathrm{N}}}{\partial\dot{q}_k} = \sum_{i=k}^{N}\left\{\left(\tau_i\hat{\boldsymbol{e}}_{i1} - \tau_{i+1}\hat{\boldsymbol{e}}_{i+1,1}\right)\cdot\hat{\boldsymbol{e}}_{k1}\right\} \tag{50}$$

$$\sum_{i=1}^{N}\boldsymbol{M}_i^a\cdot\frac{\partial\boldsymbol{\omega}^{\mathrm{B}i/\mathrm{N}}}{\partial\dot{q}_k} = \tau_k \tag{51}$$

The equations of motion for the direct-drive robot can be assembled with a mass matrix *M* and the velocity product terms *V*.

$$M\left(\Theta,\dot{\Theta}\right)\ddot{\Theta} + V\left(\Theta,\dot{\Theta}\right) = \mathrm{T} \tag{52}$$

where the joint angles, rates, and accelerations and the joint torques are the elements of the arrays $\Theta, \dot{\Theta}, \ddot{\Theta}$, and T .

As with the single link, the equations for the CMG robot share most of the terms from the equations for the direct-drive robot. The only differences are removing the applied joint torques and replacing them with a controlled internal-angular-momentum from the CMGs. The angular momentum of a link and its CMGs is given by Eq. (23). The angular momentum derivative is given by Eq. (44) added to the following CMG terms:

$$\frac{\overset{\mathrm{N}}{d}}{dt}\left(2h_r\sin\phi_i\right) = 2h_r\dot{\phi}_i\cos\phi_i\hat{\boldsymbol{e}}_{i1} + \boldsymbol{\omega}^{\mathrm{B}i/\mathrm{N}}\times 2h_r\sin\phi_i\hat{\boldsymbol{e}}_{i1} \tag{53}$$

After taking the dot product with the partial velocities, the CMG-specific terms in the equations of motion are

$$2h_r\dot{\phi}_i\cos\phi_i\hat{\boldsymbol{e}}_{i1}\cdot\hat{\boldsymbol{e}}_{k1} + \boldsymbol{\omega}^{\mathrm{B}i/\mathrm{N}}\cdot\left(2h_r\sin\phi_i\hat{\boldsymbol{e}}_{i1}\times\hat{\boldsymbol{e}}_{k1}\right), \text{ for } \mathrm{k}\le\mathrm{i} \tag{54}$$

The same *M* and *V* matrices can be used in the equations of motion with the addition of a vector of the gyroscopic coupling terms, *B*. The result is a differential equation in both Θ and the gimbal angles Φ.

$$M\left(\Theta,\dot{\Theta}\right)\ddot{\Theta} + V\left(\Theta,\dot{\Theta}\right) + B\left(\Theta,\dot{\Theta},\Phi\right) = P\left(\Theta,\Phi\right)\dot{\Phi} \tag{55}$$

where the matrix *P* is an upper-triangular matrix that reflects the alignment of an outboard scissored pair with the inboard link of interest. We show below that the form of Eq. (55) as compared to Eq. (52) results in greater differences between CMGs and direct drive than indicated by the single-link analysis.

V. Two-Link Robot

The two-link robot gives insight into the expanding design considerations for multilink robots by providing a bridge between the one degree of freedom robot discussed above and a full 3 to 6 degree of freedom robot. We discuss the interactions between the two links and how that affects the performance of the CMGs relative to direct drive. We first introduce an analogy relating the applied CMG torque to a body torque conceptually applied by the 'hand of God'. This analogy illustrates a fundamental difference between the CMGs and direct drive not seen in the single link example. We then use simulations to find robotic motions that are particularly well suited for CMGs.

A. Body Torque Analogy

With direct drive actuation, each motor moves its own link and reacts the torques produced by links further down the chain according to the angles between the joint axes—the joint topology. For a robot with parallel joint axes,

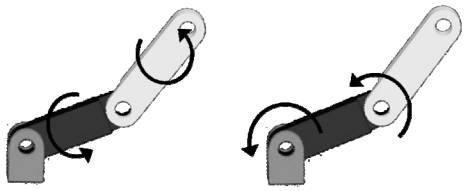

Figure 8. Body torques and joint torques.

torque applied about the second joint must be reacted by the first joint. The joint torques on perpendicular joint axes are independent because the torque is reacted against a constraint. With CMG torques, the joint axes create a zero-torque boundary condition for each link, although torque perpendicular to the joint axes does affect neighboring CMGs.

To illustrate the concept, we replace the CMGs with a phantom body torque on each link (Fig. 8). We use a subscript *j* or *b* to denote joint torques and body torques. The equations of motion in matrix form with joint torques are already given in Eq. (52). For the case of body torques, we define a parameter $\gamma_{i,j}$ as the dot product of the two joint axes.

$$\gamma_{i,j} = \hat{\mathbf{e}}_{i1} \cdot \hat{\mathbf{e}}_{j1} \tag{56}$$

The equations of motion for the body torques can be written as:

$$M\left(\Theta,\dot{\Theta}\right)\ddot{\Theta} + V\left(\Theta,\dot{\Theta}\right) = \begin{bmatrix} 1 & \gamma_{1,2} \\ 0 & 1 \end{bmatrix} \mathrm{T}_b \tag{57}$$

The matrix *P* in Eq. (55) is also an upper triangular matrix with the $\gamma_{i,j}$ multiplied by $2h_r\cos\phi_t$. Equations (52) and (57) easily permit us to write body torques in terms of joint torques:

$$\mathrm{T}_b = \begin{bmatrix} 1 & -\gamma_{1,2} \\ 0 & 1 \end{bmatrix} \mathrm{T}_j \tag{58}$$

The torque relationship does not conclude the question of joint vs. body torques. The angular velocity required to determine the power needed by each actuator also varies. Joint torques use the joint velocities—the $\dot{\theta}$s used to describe the motion of the robot. The body torques use the component of the vector $\boldsymbol{\omega}^{i/\mathrm{N}}$ along the joint axis, determined by summing up the inboard joint velocities scaled by $\gamma_{i,j}$. We can write the body velocities in terms of the joint velocities for the two link case as

$$\Theta_b = \begin{bmatrix} 1 & 0 \\ \gamma_{1,2} & 1 \end{bmatrix} \Theta_j \tag{59}$$

The power of the body torques can now be easily expressed in terms of the joint torques and velocities. For a perfectly restorative system (e.g. with only springs), we can show that the power is equal in both cases.

$$P_{b1} + P_{b2} = \Theta_j \begin{bmatrix} 1 & \gamma_{1,2} \\ 0 & 1 \end{bmatrix} \begin{bmatrix} 1 & -\gamma_{1,2} \\ 0 & 1 \end{bmatrix} \mathrm{T}_j = P_{j1} + P_{j2} \tag{60}$$

As discussed above, we are concerned with a nonconservative system. We sum the absolute value of the power at each actuator to obtain:

$$\left|P_{b1}\right| + \left|P_{b2}\right| = \left|\dot{\theta}_{j1}\right| \cdot \left|\tau_{j1} - \gamma_{1,2} \cdot \tau_{j2}\right| + \left|\gamma_{1,2} \cdot \dot{\theta}_{j1} + \dot{\theta}_{j2}\right| \cdot \left|\tau_{j2}\right| \tag{61}$$

Collecting terms, we write the power of the body torques in terms of the joint torques and an extra cross term between the rate of the first link and the joint torque on the second link.

$$\left|P_{b1}\right| + \left|P_{b2}\right| = \left|P_{j1} - \gamma_{1,2}\dot{\theta}_{j1}\tau_{j2}\right| + \left|P_{j2} + \gamma_{1,2}\dot{\theta}_{j1}\tau_{j2}\right| \tag{62}$$

This expression shows that joint torques and body torques will have different power requirements and energy demands for certain maneuvers. CMGs are an excellent means of body torque actuation, as indicated by the single-link analysis above, and may be used to exploit advantages available to the body torques. The ideas of this section also simplify the design of a multilink robot that uses CMGs and explain the results in the following section.

B. Two Link Simulations

We contrast a robot with perpendicular joint axes and a planar robot with parallel joint axes. The first could provide orientation control with two degrees of freedom (e.g., azimuth and elevation) for pointing a camera or sensor at a target. The latter provides range for reaching tasks for a manipulation robot on a spacecraft. These two cases provide two extremes of Eq. (61) with $\gamma_{1,2}$ equal to 0 or 1 (Eq. (56)).

1. Orthogonal joint axes

When the joint axes are orthogonal, not only is $\gamma_{1,2}$ equal to 0, but the equations of motion are decoupled when the second link is axisymmetric about its joint axis and the two joint axes intersect. Therefore we expect a similar power performance as for the single link. The simulations specifically offset the joint axes, translate the centers of mass, and include off-diagonal terms in the inertia matrices to expand the results in the earlier section.

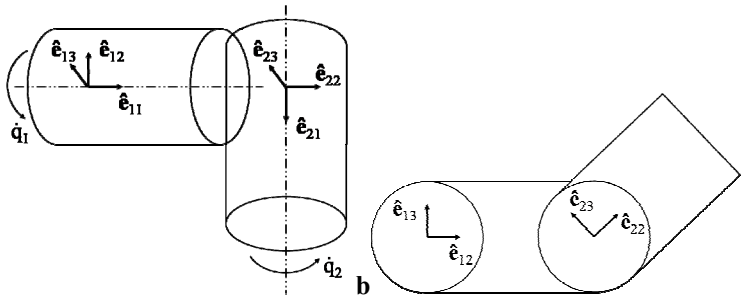

Figure 9. Joint topologies. a) *Perpendicular joint axes.* **b)** *Parallel joint axes.*

The asymmetry of the second link combines with misalignment of the axes to introduce fluctuations of the system angular momentum that affect CMG sizing. The CMGs on the inner link must account for the angular momentum of both the inner and outer link taken about the first joint axis. The CMGs on the second link need only conserve angular momentum of the second link about its joint axis (because an inertial base is assumed). However, the net angular velocity includes a component from the first joint velocity that can project along the second joint axis, even when the axes are perpendicular. The CMGs on a multi-link robot could be sized according to the expected maximum angular momentum about each joint, with larger CMGs on the inner link and smaller CMGs on the outer link. An economic alternative is to place identical CMGs on each link and adjust the maximum joint velocity so that the net angular momentum is bounded by the capacity of the CMGs. We opt for the latter option in this work. We calculate the angular velocities of the joints corresponding to the maximum angular momentum about each joint and solve for the maximum angular velocities that will not saturate the CMGs. For this exploratory study, we arbitrarily set the peak acceleration and jerk to the same numerical value as the peak angular velocity to satisfy Eq. (35) while limiting the contribution of maximum jerk to the gimbal acceleration and power cost (cf. Eqs. (29) and (14)). The angle of rotation and time to accomplish the maneuver are given by Eqs. (36) and (37). The start time of the rotations are offset by Δt_0, a parameter randomly assigned to either the first- or second-link maneuver with the other link starting at t=0. The parameters used for a 1000 trial simulation are given in Table 2. The principal inertias, center-of-mass offset, and joint axis locations are randomly assigned component-wise from a uniform distribution over the range given in Table 2. We use a uniform distribution to perform an exploratory analysis, not to assign statistical distributions to the outputs. The maximum inertia about the joint axis, the peak body rate, and peak gimbal angle are calculated and given in Table 2.

Table 2. Parameter value ranges for two link simulations. *All other parameters use the baseline values given in Table 1. Joint axes are orthogonal to each other. Energy change is the range after 1000 simulations*

	Parameters		Inputs				
	I_{gr}, kg·m^2	h_r, N·m·s	$I_{b,ii}$, kg·m^2	r(i), m	l_1(i), m	Δt_0, s	sign($\Delta\theta$)
Ortho	0.1	0.53	0.8–1.2	-0.5–0.5	-1–1	0–4	+/-
Parallel	0.1	0.53	0.8–1.2	-0.5–0.5	-1–1	0–4	+/-

	Intermediate calculations				Result
	$\omega_{\max}$, s^{-1}	I_{max}, kg·m^2	ϕ_{peak}, deg	$\Delta\theta$, deg	*PED*, %
Ortho	0.1–0.5 0.6–1.2	1.9–6.1 0.8–1.6	7–74 50–80	10–59 65–134	0–33
Parallel	0.03–1.0 0.0–0.9	1.0–4.0 0.9–1.5	3–73 1–73	4-112 0.2–98	-49–38

Figure 10 plots the *PED* calculated for both links together against the peak gimbal angle of the first link, ϕ_{1peak}. The greater inertia about the first joint axis causes the first link's gimbal angle to influence *PED* more than the second link's gimbal angle. Although not shown here, the combined inertia of both links affects the relative performance of CMGs. The combined inertia of both links varies with time and determines the angular momentum about the first joint axis (and ϕ_{1peak}). Therefore we only show *PED* vs. ϕ_{1peak}. As with the single link robot, the *PED*

is greater than zero with some dependence on the size of the CMG as represented by the peak angle for the first gimbal. The *PED* values for two links are greater than for the single link because of the interplay between the increased body inertia relative to jerk (cf. Eqs. (29) and (14)).

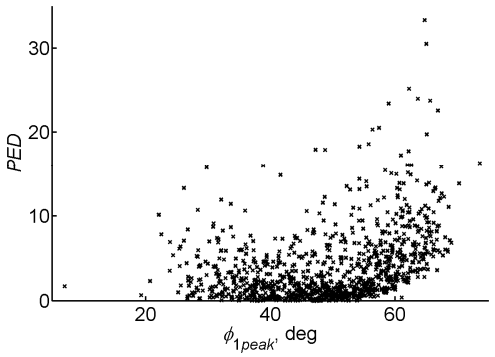

Figure 10. Relative performance of CMGs and direct drive for two orthogonal links.

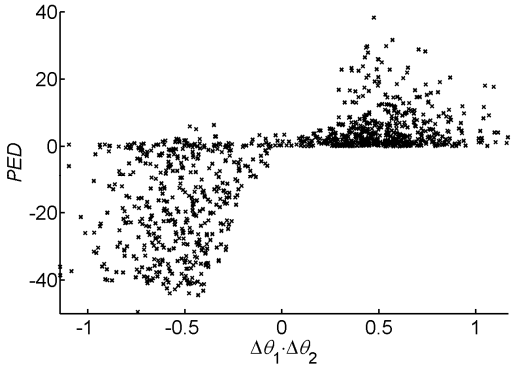

Figure 11. The joint-angle product determines if CMGs use less energy than direct drive for parallel-joint-axes robots.

2. Parallel joint axes

None of the simulations thus far have indicated a compelling advantage of CMGs over direct drive or a basic joint motor. A two link robot with parallel axes takes advantage of the fundamental differences in how torque is applied to each link as discussed in section V.A. We continue to use identical CMGs on each link and adjust the maximum joint rate accordingly. For parallel joint axes, the sign of each joint's rotation is critical in determining the maximum joint rate (cf. Eq. (59)). When both joints move together, the second link saturates its CMGs more easily because both joint velocities add to determine the link's angular momentum. When the joints move in opposite directions, the second link can attain a high joint rate while keeping the angular momentum low. We calculate the maximum joint velocities according to the sign of the desired rotations. Zero velocity of either link is also possible due to the start-time offset Δt_0 and may be the limiting case in selecting maximum joint velocity.

For 1000 trials over the same range of parameters as the orthogonal-axes case, the *PED* is less than zero for 403 trials. A key indicator of the *PED* is the product of the joint angles (Fig. 11)—in particular the sign agreement of the angles. This shows that CMGs are more efficient than direct drive when the joints move in opposite directions—as they must for reaching tasks. Direct drive is better when the joints move together—typical for moving an item across the robot's field of view.

VI. Conclusion

This study explores potential advantages of CMGs over direct drive as robotic actuators. We review CMG dynamics for a robotic system with a focus on the gimbal torque and power required to produce a given body rate. The analysis of the CMG dynamics also provides an expression for peak gimbal rates—a useful design tool for sizing gimbal motors. We use a scissored pair on each robotic link aligned with the joint axis to minimize off-axis torques and to mitigate the power costs due to off-axis body rotation. A simple expression for the power used by the scissored pair in rotating a single body shows that power for direct-drive actuation is equal to power for CMGs. Gimbal inertia, CMG saturation singularities, and link inertia and jerk hurt performance when not carefully considered. Simulations that include transverse rotations indicate that relative power use depends on these factors rather than the transverse rotation. When sizing gimbal motors, peak gimbal torques and rates can be easily estimated from simple equations arising from CMG dynamics and conservation of momentum.

We develop recursive equations of motion for a general n-link robot to facilitate simulation. For a two-link robot, CMGs can provide an advantage in power use because the exchange of momentum between the CMGs and the body acts as a body torque rather than a joint torque. This advantage depends on the angle between adjacent joint axes, with parallel joint axes preferred, and whether the joints rotate in the same or opposite directions. CMGs are better suited for reaching radially from the base, while direct drive is better for panning across ones field of view relative to the base. The scissored-pair CMG system provides reactionless actuation of a robot at a power cost comparable to direct drive actuation, a promising combination for future use of CMGs in non-traditional applications.

Acknowledgments

D. Brown was supported by an NSF IGERT grant.

The author also thanks Dr. Mason Peck and his lab at Cornell University for additional funding and equipment and many excellent discussion, with special thanks to Michele Carpenter whose work in this area both inspired and directed my efforts.

References

[1] Billing-Ross, J.A., and Wilson, J.F., "Pointing System Design for Low-Disturbance Performance," AIAA Guidance, Navigation, and Control Conference, Vol. 1, AIAA, Washington, DC, 1988, pp. CP4106-444-451.

[2] Schaub, H., Vadali, S.R., and Junkins, J.L., "Feedback control law for variable speed control moment gyros," Journal of the Astronautical Sciences, Vol. 46, No. 3, 1998, pp. 307-328.

[3] Wie, B., "Space Vehicle Dynamics and Control," AIAA Education Series, AIAA, Washington, DC, 2008,

[4] Lappas, V.J., Steyn, W.H., and Underwood, C.I., "Attitude Control for Small Satellites Using Control Moment Gyros," Acta Astronautica, Vol. 51, No. 1-9, 2002, pp. 101-111.

[5] Wie, B., Bailey, D., and Heiberg, C., "Rapid Multitarget Acquisition and Pointing Control of Agile Spacecraft," Journal of Guidance, Control, and Dynamics, Vol. 25, No. 1, 2002, pp. 96-104.

[6] Peck, M.A., "Low-Power, High-Agility Space Robotics," AIAA Guidance, Navigation, and Control Conference, AIAA, Washington, DC, 2005, pp. CP6243.

[7] Romano, M., and Agrawal, B.N., "Attitude Dynamics/Control of Dual-Body Spacecraft with Variable-Speed Control Moment Gyros," Journal of Guidance, Control, and Dynamics, Vol. 27, No. 4, 2004, pp. 513-525.

[8] Yang, L.F., Mikulas, M.M., Jr, Park, K.C., "Slewing Maneuvers and Vibration Control of Space Structures by Feedforward/Feedback Moment-Gyro Controls," Journal of Dynamic Systems, Measurement, and Control, Vol. 117, 1995, pp. 343-351.

[9] Carpenter, M.D., and Peck, M.A., "Dynamics of a High-Agility, Low-Power Imaging Payload," IEEE Transactions on Robotics, 2008 (To appear),

[10] Crenshaw, J.W., "2-SPEED, A Single-Gimbal Control Moment Gyro Attitude Control System," AIAA Guidance and Control Conference, AIAA, Washington, DC, 1973, pp. CP895.

[11] Aubrun, J.N., and Margulies, G., "Gyrodampers for Large Space Structures," NASA, 159171, 1979.

[12] Havill, J.R., and Ratcliff, J.W., "A Twin-Gyro Attitude Control System for Space Vehicles," Tech. Rep. NASA TN D-2419, 1964,

[13] Brown, D., and Peck, M.A., "Scissored-Pair Control Moment Gyros: A Mechanical Constraint Saves Power," Journal of Guidance, Control, and Dynamics, to appear,

[14] Liska, D., "A Two-Degree-of-Freedom Control Moment Gyro for High-Accuracy Attitude Control," Journal of Spacecraft and Rockets, Vol. 5, No. 1, 1968, pp. 74-83.

[15] Schaub, H., and Junkins, J.L., "Analytical Mechanics of Space Systems," American Institute of Aeronautics and Astronautics, Inc., Reston, Virginia, 2003, pp. 438-440.

[16] Kurokawa, H., "Survey of Theory and Steering Laws of Single-Gimbal Control Moment Gyros," Journal of Guidance, Control, and Dynamics, Vol. 30, No. 5, 2007,

[17] Lappas, V.J., Steyn, W.H., and Underwood, C.I., "Torque Amplification of Control Moment Gyros," Electronics Letters, Vol. 38, No. 15, 2002, pp. 837-839.

[18] Peck, M.A., "Uncertainty Models for Physically Realizable Inertia Dyadics," The Journal of the Astronautical Sciences, Vol. 54, No. 1, 2006,

[19] Kane, T.R., and Levinson, D.A., "Dynamics: Theory and Applications," McGraw-Hill, New York, 1985,

[20] Kane, T.R., and Levinson, D.A., "The Use of Kane's Dynamical Equations in Robotics," The International Journal of Robotics Research, Vol. 2, No. 3, 1983, pp. 3-21.

[21] Moon, F.C., "Applied Dynamics: With Applications to Multibody and Mechatronic Systems," Wiley, New York, 1998, pp. 270.